Three-Dimensional Multiple-Scattering Technique for the Analysis of Photonic-Crystal Slabs

Stefano Boscolo and Michele Midrio

***Abstract*—A numerical technique allowing theoretical analysis of propagation in three-dimensional (3-D) photonic-crystal (PC) slabs is presented. The method is an extension to the 3-D case of the two-dimensional multiple-scattering technique that was originally developed by Tayeb and Maystre. As an application, the method is used to numerically estimate the out-of-plane scattering losses in a straight PC waveguide of finite height.**

***Index Terms*—Electromagnetic scattering, numerical analysis, optical waveguides, periodic structures, photonic crystals.**

I. Introduction

PHOTONIC CRYSTALS have attracted much interest due to their potential for controlling the propagation of light [1]–[6]. Owing to the complexity of the geometries that are customarily used, most of the theoretical work done so far has been based on numerical investigations. Availability of efficient and reliable numerical codes is then a key issue for accurate modeling of photonic crystals (PCs), and this becomes particularly important if the behavior of a real three-dimensional (3-D) structure has to be analyzed.

Mainly, so far, 3-D simulations have been performed with the following numerical techniques: the finite-difference time-domain technique (FDTD) [7], the Green's tensor approach [8], and the Fourier-modal method [9].

The first of these techniques works in the time domain, while the others work in the frequency domain. Despite this difference, these methods share a common concept, which raises similar pros and cons. As a matter of fact, in those techniques, the starting point is *discretization* of the computational domain, or of a part of it. This makes the codes very broad in scope: in fact, since any object may be discretized, the numerical techniques may operate with any kind and shape of dielectrics in the PC. The price to pay for this wide generality is memory allocation and computational time. Indeed, the code accuracy improves with the number of samples that are used to discretize the objects in the PC.

This paper aims at illustrating an alternative numerical method that may be used to perform theoretical investigations of PCs, with a possibly reduced memory occupancy and computational time. The method is based on a different approach with respect to those previously mentioned. Indeed, the aim is not at developing a code that may operate with any geometry; rather, the focus is on the kind of structure that is illustrated in Fig. 1: a multilayer structure that, in its most general form, may comprise a substrate, an insulating buffer, the lower cladding, the waveguide core, the upper cladding, and, due to computational reasons, an air and a perfectly matched layer (PML) above the structure top face [10]. In a typical configuration, a two-dimensional (2-D) lattice of holes is etched into this layered medium.

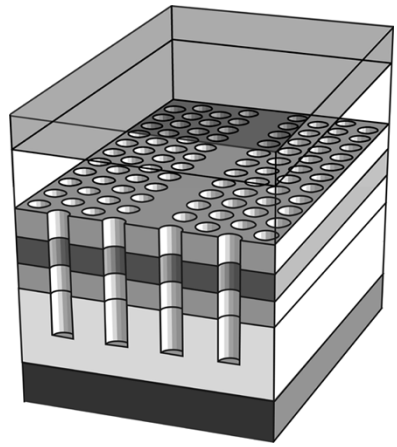

Fig. 1. Schematic diagram of a PC waveguide.

Essentially, this paper will then deal with planar slabs and cylindrical holes and will fully exploit the fact that these objects are geometrically "simple" to *rigorously solve* the Maxwell's equations in analytical form.

The basic idea is the following. To describe the field inside or around a cylindrical object, the best choice is to write the field as a sum of the "natural" modes of cylindrical objects, the *cylindrical harmonics*. With this choice, there is no need to make any discretization, and it may be reasonably expected that a few terms will be sufficient to properly approximate the field. Indeed, this has been shown to happen in the 2-D case, where the multiple-scattering technique proposed in [11] is one of the most powerful, fastest, and most accurate simulation tools available so far.

The method discussed in the present paper is an extension of the 2-D scattering code to the 3-D case, and the problem that must be solved is the following: a given field is injected into a PC waveguide that comprises a number of arbitrarily located air holes, and a routine is developed to compute the field that is scattered by the ensemble of holes, as well as the field that is transmitted into each of them.

Manuscript received January 27, 2004; revised May 26, 2004. This work was performed in the framework of the European Project "PICCO" (Photonic Integrated Circuits using Crystal Optics) under IST-1999-10361 and under the Italian FIRB Project "Metodi e modelli numerici di dispositivi fotonici per reti ad alta capacità."

The authors are with the Istituto Nazionale per la Fisica della Materia (INFM), Dipartimento di Ingegneria Elettrica, Gestionale e Meccanica, Università degli Studi di Udine, Udine 33100, Italy (e-mail: midrio@uniud.it).

Digital Object Identifier 10.1109/JLT.2004.833276

The paper is organized as follows. Section II begins with the simple case of a single hole etched in the layered structure. Later on, Section III generalizes the theory to the scattering from an arbitrary number of holes. Section IV reports the results of some tests performed to check the routine convergence and accuracy. These refer to computation of out-of plane scattering losses from a PC membrane. Some concluding remarks will close the paper.

II. 3-D Scattering From a Single Etched Hole

With reference to the structure of Fig. 1, we identify *two different layered regions*. The first, referred to as the "slab," is the region formed by the stack of dielectric media that make up the slab waveguide in the absence of the holes (plus the air and the PML layer above the waveguide top surface).

The second region, referred to as the "hole," is the cylindrical region that contains one of the air holes and that goes from the upper to the lower computational edges (see Fig. 2).

Let us now consider the scattering of an incident field from a single etched hole. Three electromagnetic (EM) fields are involved in the process: the incident field, which we suppose to be assigned *a priori*, the scattered field, and the field that is transmitted into the hole, which we denote as $\{\mathbf{E}^{(i)},\mathbf{H}^{(i)}\}$, $\{\mathbf{E}^{(s)},\mathbf{H}^{(s)}\}$, and $\{\mathbf{E}^{(t)},\mathbf{H}^{(t)}\}$, respectively.

The three fields obey continuity conditions on the lateral surface of the cylinder that contains the hole, i.e., they satisfy

$$\begin{cases} \left(\mathbf{E}^{(i)}+\mathbf{E}^{(s)}\right)\times\hat{\boldsymbol{r}}=\mathbf{E}^{(t)}\times\hat{\boldsymbol{r}}, \\ \left(\mathbf{H}^{(i)}+\mathbf{H}^{(s)}\right)\times\hat{\boldsymbol{r}}=\mathbf{H}^{(t)}\times\hat{\boldsymbol{r}}. \end{cases} \quad r=\rho \tag{1}$$

with ρ being the cylinder radius. We now show explicitly how these equations may be turned into an an efficient numerical routine.

A. Incident Field

In order to represent the incident field in a proper way, we use a result that we prove in Appendix A: the whole EM field of a layered region (such as the *slab region* in which the incident field propagates) is uniquely determined once its $\hat{\boldsymbol{z}}$-directed components are specified.

Therefore, the incident field is completely described if we only set the values of $E_z^{(i)}$ and $H_z^{(i)}$, which we respectively write as

$$E_z^{(i)}=-\sum_{\ell,m}T_{\ell,m}^{(i)}\frac{\left(\chi_{\mathrm{SL}m}^{(\mathrm{TM})}\right)^2 e^{i\ell\varphi}}{n_{\mathrm{SL}}^2(z)\epsilon_0}J_\ell\left(\chi_{\mathrm{SL}m}^{(\mathrm{TM})}r\right)\mathcal{E}_m^{(\mathrm{SL})}(z)$$

$$H_z^{(i)}=\sum_{\ell,p}L_{\ell,p}^{(i)}\frac{\left(\chi_{\mathrm{SL}p}^{(\mathrm{TE})}\right)^2 e^{i\ell\varphi}}{\mu_0}J_\ell\left(\chi_{\mathrm{SL}p}^{(\mathrm{TE})}r\right)\mathcal{H}_p^{(\mathrm{SL})}(z).$$

Here, and in the equations herafter, the origin of the coordinate system is in the center of the hole. Moreover, $T_{\ell,m}^{(i)}$ and $L_{\ell,m}^{(i)}$ are expansion coefficients, which have to be regarded as known coefficients as soon as the shape of the incident field is assigned. Whereas $n_{\mathrm{SL}}(z)$ is the index distribution in the slab region, $\chi_{\mathrm{SL}m}^{(\mathrm{TM})}$ and $\chi_{\mathrm{SL}p}^{(\mathrm{TE})}$ are the radial wavenumbers for the mth TM and the pth TE mode of the slab region, respectively.

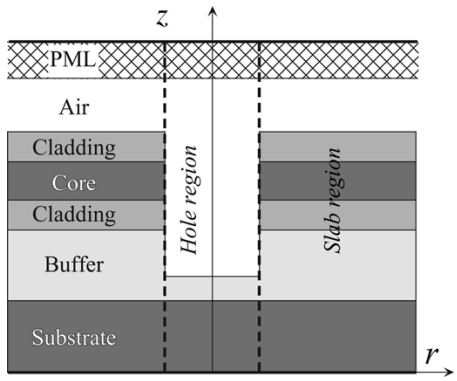

Fig. 2. Cross section of a PC slab with a single hole.

Finally, $J_\ell(\cdot)$ is the J-type Bessel function of order ℓ, and $\mathcal{E}_m^{(\mathrm{SL})}$, $\mathcal{H}_p^{(\mathrm{SL})}$ are the field profiles along z for the mth TM mode and the pth TE mode of the slab region, respectively. The explicit form of these function, along with the values of the modes' radial wavenumbers, are given in Appendix A.

B. Diffracted and Excited Fields

In an analogous fashion, these fields also are completely specified once their $\hat{\boldsymbol{z}}$-directed components are given, and these may be written as

$$E_z^{(s)}=-\sum_{\ell,m}T_{\ell,m}^{(s)}\frac{\left(\chi_{\mathrm{SL}m}^{(\mathrm{TM})}\right)^2 e^{i\ell\varphi}}{n_{\mathrm{SL}}^2(z)\epsilon_0}H_\ell^{(2)}\left(\chi_{\mathrm{SL}m}^{(\mathrm{TM})}r\right)\mathcal{E}_m^{(\mathrm{SL})}(z)$$

$$E_z^{(t)}=-\sum_{\ell,p}T_{\ell,p}^{(t)}\frac{\left(\chi_{\mathrm{HO}p}^{(\mathrm{TM})}\right)^2 e^{i\ell\varphi}}{n_{\mathrm{HO}}^2(z)\epsilon_0}J_\ell\left(\chi_{\mathrm{HO}p}^{(\mathrm{TM})}r\right)\mathcal{E}_p^{(\mathrm{HO})}(z)$$

and

$$H_z^{(s)}=\sum_{\ell,m}L_{\ell,m}^{(s)}\frac{\left(\chi_{\mathrm{SL}m}^{(\mathrm{TE})}\right)^2 e^{i\ell\varphi}}{\mu_0}H_\ell^{(2)}\left(\chi_{\mathrm{SL}m}^{(\mathrm{TE})}r\right)\mathcal{H}_m^{(\mathrm{SL})}(z)$$

$$H_z^{(t)}=\sum_{\ell,p}L_{\ell,p}^{(t)}\frac{\left(\chi_{\mathrm{HO}p}^{(\mathrm{TE})}\right)^2 e^{i\ell\varphi}}{\mu_0}J_\ell\left(\chi_{\mathrm{HO}p}^{(\mathrm{TE})}r\right)\mathcal{H}_p^{(\mathrm{HO})}(z)$$

respectively.

Here, $H_\ell^{(2)}(\cdot)$ is the second-type Hankel function of order ℓ, while $L_{\ell,p}^{(s)}$, $T_{\ell,p}^{(s)}$, $L_{\ell,p}^{(i)}$, and $T_{\ell,p}^{(i)}$ are the expansion coefficients that have to be determined in order for the problem to be numerically solved. Subscripts (HO) and (SL) were used to denote the "hole" and "slab" regions, respectively.

C. The Numerical Routine

The basic idea to turn continuity conditions into a numerical routine is the same as in the mode-matching technique [13]. We use the same number of modes to expand the field in both the slab and the hole region, and we compute the projection of the continuity conditions on each mode of the slab region. For instance, if we take the inner product of the first of (1) with the magnetic field of each mode of the slab region, and the inner product of the electric field of each slab mode with the second

of (1), and exploit the orthogonality relationships reported in Appendix A, the following system of linear equations is found:

$$\left[\begin{array}{c|c|c|c} \mathsf{M}_{11} & 0 & \mathsf{M}_{13} & \mathsf{M}_{14} \\ \hline 0 & \mathsf{M}_{22} & 0 & \mathsf{M}_{24} \\ \hline \mathsf{M}_{31} & 0 & \mathsf{M}_{33} & 0 \\ \hline 0 & \mathsf{M}_{42} & \mathsf{M}_{43} & \mathsf{M}_{44} \end{array}\right] \left[\begin{array}{c} \mathbf{L}_\ell^{(s)} \\ \hline \mathbf{T}_\ell^{(s)} \\ \hline \mathbf{L}_\ell^{(t)} \\ \hline \mathbf{T}_\ell^{(t)} \end{array}\right] = \left[\begin{array}{c} \mathbf{P}_1 \\ \hline \mathbf{P}_2 \\ \hline \mathbf{P}_3 \\ \hline \mathbf{P}_4 \end{array}\right]. \tag{2}$$

Notice that this system actually expresses continuity of the Poynting vector through the lateral surface of the cylinder. Therefore, since the modes in both the slab and the hole regions are orthogonal to each other, the continuity, in fact, arises from the principle of energy conservation.

In (2), $\mathbf{L}_\ell^{(s)}$ is a column vector that contains the unknown coefficients for the ℓth azimuthal order of the transverse-electric (TE) diffracted field. The column length is equal to the number $m_{\max}$ of radial modes that are used to expand the field with respect to z, both in the hole and in the hosting slab guide. In an analogous fashion, vector $\mathbf{T}_\ell^{(s)}$ contains the expansion coeffcients for the ℓth azimuthal order of the transverse-magnetic (TM) diffracted field. Finally, $\mathbf{L}_\ell^{(t)}$ and $\mathbf{T}_\ell^{(t)}$ contain the expansion coefficients for the fields that are transmitted into the hole.

M_{ij} are $m_{\max} \times m_{\max}$ square matrices, whose entries are listed in Appendix B. On the other hand, $\mathbf{P}_i$ are column vectors of length $m_{\max}$ that depend on the expansion coefficients of the incident field. They also are listed in Appendix B.

The scattering problem has thus been turned into the problem of solving a nonhomogenous system of $4m_{\max}$ linear equations with $4m_{\max}$ unknowns for *each of the azimuthal modes* that are used in the field expansion.

Notice that, in general, the scattered and the excited fields are *hybrid* fields, i.e., they are neither purely TE nor purely TM, even if the incident field is either TE or TM. In other words, the polarization of the incident field is not preserved in the scattering process. As a matter of fact, for a purely TE (or TM) field to exist, the system of continuity (2) must split into two subsystems, one involving the T expansion coefficients only, and the other involving the L coefficients only. Looking at the matrix entries in Appendix B, it is easy to check that this only occurs when the azimuthal order $\ell = 0$ (in fact, in this case, $\mathsf{M}_{12} = \mathsf{M}_{14} = \mathsf{M}_{31} = \mathsf{M}_{33} = 0$). Hence, unless the incident field has the only $\ell = 0$ harmonic, the scattered and excited fields contain both TE and TM components.

The reader may recognize that this feature is not peculiar of the problem we are dealing with. Indeed, it is shared by other propagation problems where continuity conditions are imposed on the boundaries between dielectric materials. For instance, the modes of optical fibers are purely TE or purely TM only for the azimuthal order $\ell = 0$, while they become hybrid HE or EH modes for any $\ell \neq 0$ [15].

D. Scattering and Transmission Matrices

Before we turn to the case of the propagation through an arbitrary number of cylinders, we briefly illustrate how the system (2) may be rewritten in an alternative form that allows us to nicely define a scattering and a transmission matrix for the dielectric arrangement with which we have been dealing. To this end, it suffices to notice that if we formally rewrite the right-hand side (RHS) of (2) as

$$\left[\begin{array}{c} \mathbf{P}_1 \\ \hline \mathbf{P}_2 \\ \hline \mathbf{P}_3 \\ \hline \mathbf{P}_4 \end{array}\right] = \left[\begin{array}{c|c} \mathsf{P}_{11} & 0 \\ \hline 0 & \mathsf{P}_{22} \\ \hline \mathsf{P}_{31} & 0 \\ \hline 0 & \mathsf{P}_{42} \end{array}\right] \cdot \begin{bmatrix} \mathbf{L}_\ell^{(i)} \\ \mathbf{T}_\ell^{(i)} \end{bmatrix} \tag{3}$$

the whole system becomes equivalent to the combination of the following two systems

$$\mathbf{V}_\ell = \mathsf{S}_\ell \mathbf{U}_\ell, \quad \mathbf{W}_\ell = \mathsf{T}_\ell \mathbf{U}_\ell \tag{4}$$

where

$$\mathbf{V}_\ell = \begin{bmatrix} \mathbf{L}_\ell^{(s)} \\ \mathbf{T}_\ell^{(s)} \end{bmatrix}, \quad \mathbf{U}_\ell = \begin{bmatrix} \mathbf{L}_\ell^{(i)} \\ \mathbf{T}_\ell^{(i)} \end{bmatrix}, \quad \mathbf{W}_\ell = \begin{bmatrix} \mathbf{L}_\ell^{(t)} \\ \mathbf{T}_\ell^{(t)} \end{bmatrix} \tag{5}$$

and S_ℓ and T_ℓ are suitable $2m_{\max} \times 2m_{\max}$ square matrices. Matrices P_{ij} are defined in Appendix B.

Equation (4) defines the scattering and the transmission matrices of the cylinder embedded in the slab waveguide. Indeed, S_ℓ relates the coefficients of the scattered field to those of the incident field, whereas T_ℓ relates the field that is transmitted into the cylinder to the incident field.

III. 3-D Scattering From an Arbitrary Number of Cylinders

We now turn to the case of propagation through a set of $N > 1$ cylinders embedded in the slab waveguide. The starting point is still the set of continuity conditions to which the field must obey. Those now read as

$$\begin{cases} \left(\mathbf{E}^{(i)} + \mathbf{E}_p^{(s)} + \sum\limits_{q \neq p} \mathbf{E}_q^{(s)}\right) \times \hat{\boldsymbol{r}}_p = \mathbf{E}_p^{(t)} \times \hat{\boldsymbol{r}}_p \\ \left(\mathbf{H}^{(i)} + \mathbf{H}_p^{(s)} + \sum\limits_{q \neq p} \mathbf{H}_q^{(s)}\right) \times \hat{\boldsymbol{r}}_p = \mathbf{H}_p^{(t)} \times \hat{\boldsymbol{r}}_p \end{cases} \tag{6}$$

where $\{\mathbf{E}_p^{(s)}, \mathbf{H}_p^{(s)}\}$ and $\{\mathbf{E}_p^{(t)}, \mathbf{H}_p^{(t)}\}$ are the EM fields that are scattered by and transmitted into the pth cylinder, respectively, and $\hat{\boldsymbol{r}}_p$ is the unit vector of the radial coordinate of the cylindrical reference frame that is centred in the pth cylinder.

The conditions have to be applied at each $|\mathbf{r}_p| = \rho_p$, with ρ_p being the radius of the pth cylinder, and for any $p = 1, \ldots, N$.

Passing from the single to the multiple-scattering case is then a formally and conceptually simple task. Still, one should notice that in order to make computation of (6) really feasible, the expressions of $\mathbf{E}_q^{(s)}$ and $\mathbf{H}_q^{(s)}$ in the pth cylindrical reference frame are required. Those may be computed by writing the qth cylinder Debye's potentials (which entirely defines the field in

the qth hole, see Appendix A) through the Graf's addition formula (see [12, eq. (9.1.79)]. For instance, the TE potential for the qth mode of the slab may be written as

$$\begin{aligned}\mathcal{L}_q &= e^{i\ell\varphi_q} H_\ell^{(2)}\left(\chi_{\mathrm{SL}m}^{(\mathrm{TE})} r_q\right)\mathcal{H}_m(z)\\ &= \sum_k \left(e^{i(k-\ell)\theta_{qp}} H_{\ell-k}^{(2)}\left(\chi_{\mathrm{SL}m}^{(\mathrm{TE})} d_{qp}\right)\right)\\ &\quad \cdot e^{ik\varphi_p} J_k\left(\chi_{\mathrm{SL}m}^{(\mathrm{TE})} r_p\right)\mathcal{H}_m(z)\end{aligned} \tag{7}$$

where d_{qp} is the distance between the centers of cylinders p and q, and θ_{qp} is the azimuthal coordinate of the center of cylinder q in the reference frame of cylinder p, respectively. A similar expression holds for potential $\mathcal{T}_q$, which defines the TM mode as well.

Two facts are noteworthy.

1) Graf's formula couples the terms with different azimuthal orders, and this implies a major difference between the cases of the single hole and that of the arbitrary number of holes. Indeed, suppose that the field expansion is made on azimuthal orders that range from $-\ell_{\max}$ to $\ell_{\max}$. As we have shown previously, in the case of a single scatterer, the whole EM problem might be turned into the solution of $2\ell_{\max}+1$ decoupled linear systems, one for each of the azimuthal orders that had been used in the field expansion, whereas in the multiple-scattering case, there will be one single system to be solved, and it will contain all the azimuthal orders.
2) As for the radial wavenumbers, Graf's formula acts in the opposite way. Indeed, it does not couple terms with different wavenumbers. As we show hereafter, this is an important fact because it allows reduction of the whole scattering problem to the form of a *sparse system* of linear equations. To prove this statement, we may proceed in the same way as in the single cylinder case, first verifying that (6) is equivalent to the combination of the linear systems

$$\mathbf{V}^{[p]} = \mathsf{S}^{[p]} \cdot \left(\mathbf{U}^{[p]} + \sum_{q\neq p} \mathsf{B}_{pq} \cdot \mathbf{V}^{[q]}\right), \quad p=1,\ldots,N \tag{8}$$

$$\mathbf{W}^{[p]} = \mathsf{T}^{[p]} \cdot \left(\mathbf{U}^{[p]} + \sum_{q\neq p} \mathsf{B}_{pq} \cdot \mathbf{V}^{[q]}\right), \quad p=1,\ldots,N \tag{9}$$

which generalize (5) to the case of more than a single scatterer.

The following notation was introduced: $\mathbf{V}^{[q]}$ denotes the whole set of the coefficients for the field which is scattered by the qth cylinder, namely

$$\mathbf{V}^{[q]} = \left[\mathbf{V}_{-\ell_{\max}}^{[q]} \ldots \mathbf{V}_0^{[q]} \ldots \mathbf{V}_{\ell_{\max}}^{[q]}\right]^{\mathrm{T}}.$$

Each of the $\mathbf{V}_\ell^{[q]}$ has the same form as in (5). In addition

$$\mathsf{S}^{[p]} = \mathrm{diag}\left\{\mathsf{S}_{-\ell_{\max}}^{[p]}, S_{-\ell_{\max}+1}^{[p]}, \ldots, \mathsf{S}_{\ell_{\max}-1}^{[p]}, \mathsf{S}_{\ell_{\max}}^{[p]}\right\}$$

is a block diagonal matrix, with each of the $\mathsf{S}_\ell^{[p]}$ as in (4). Finally, B_{pq} are $[2m_{\max}(2\ell_{\max}+1) \times 2m_{\max}(2\ell_{\max}+1)]$ squared fringed matrices with the form

$$\mathsf{B}_{pq} = \begin{bmatrix} \mathsf{H}_0 & \mathsf{H}_1 & \cdots & \mathsf{H}_{2\ell_{\max}} \\ \mathsf{H}_{-1} & \mathsf{H}_0 & & \vdots \\ & \ddots & & \vdots \\ \vdots & & \mathsf{H}_0 & \mathsf{H}_1 \\ \mathsf{H}_{-2\ell_{\max}} & \cdots & \mathsf{H}_{-1} & \mathsf{H}_0 \end{bmatrix} \tag{10}$$

where, due to the fact that Graf's formula does not couple terms with different radial wavenumbers, H_ℓ is a $2m_{\max} \times 2m_{\max}$ diagonal matrix, with the diagonal elements as follows:

$$\begin{aligned}\mathsf{H}_\ell = \mathrm{diag}\Big\{&H_\ell^{(2)}\left(\chi_{\mathrm{SL}_1}^{(\mathrm{TE})} d_{pq}\right), \ldots, H_\ell^{(2)}\left(\chi_{\mathrm{SL}_{m_{\max}}}^{(\mathrm{TE})} d_{pq}\right)\\ &H_\ell^{(2)}\left(\chi_{\mathrm{SL}_1}^{(\mathrm{TM})} d_{pq}\right), \ldots, H_\ell^{(2)}\left(\chi_{\mathrm{SL}_{m_{\max}}}^{(\mathrm{TM})} d_{pq}\right)\Big\} e^{-ir\theta_{qp}}.\end{aligned}$$

Let us now consider (8) and rewrite it as

$$\mathsf{A} \cdot \overline{\mathbf{V}} = \hat{\mathbf{U}} \tag{11}$$

where

$$\overline{\mathbf{V}} = \left[\mathbf{V}^{[1]}, \mathbf{V}^{[2]}, \ldots, \mathbf{V}^{[N]}\right]^{\mathrm{T}}$$

and the matrix

$$\mathsf{A} = \mathsf{I} - \mathsf{S} \cdot \mathsf{B} \tag{12}$$

with I the identity matrix and

$$\mathsf{B} = \begin{bmatrix} 0 & \mathsf{B}_{12} & \cdots & \mathsf{B}_{1N} \\ \mathsf{B}_{21} & 0 & & \mathsf{B}_{2N} \\ \vdots & & \ddots & \vdots \\ \mathsf{B}_{N1} & \mathsf{B}_{N2} & \cdots & 0 \end{bmatrix}$$

$$\mathsf{S} = \begin{bmatrix} \mathsf{S}^{[1]} & 0 & \cdots & 0 \\ 0 & \mathsf{S}^{[2]} & & 0 \\ \vdots & & \ddots & \vdots \\ 0 & 0 & \cdots & \mathsf{S}^{[N]} \end{bmatrix}.$$

Finally

$$\hat{\mathbf{U}} = \left[\mathsf{S}^{[1]}\mathbf{U}^{[1]}, \mathsf{S}^{[2]}\mathbf{U}^{[2]}, \ldots, \mathsf{S}^{[N]}\mathbf{U}^{[N]}\right]^{\mathrm{T}}.$$

Notice that all the matrices in the RHS of (12) are sparse matrices, but matrix A itself is not. Nonetheless, no large memory occupancy is actually required to solve the linear system (11) if an iterative solution routine is used. Indeed, in any iterative procedure (conjugate gradient, biconjugate gradient, etc.), explicit knowledge of matrix A is not actually needed [14]. Rather, computation of matrix–vector products such as $\mathsf{A} \cdot \overline{\mathbf{V}}_n$ or $\mathsf{A}^T \cdot \overline{\mathbf{V}}_n$ has to be performed at each iteration. $\overline{\mathbf{V}}_n$ is the solution at step n. In our case, it turns out that

$$\mathsf{A}\overline{\mathbf{V}}_n = \overline{\mathbf{V}}_n - \mathsf{S} \cdot (\mathsf{B}\overline{\mathbf{V}}_n)$$

and therefore we may proceed as follows. We only store the sparse matrices B and S. At each step of the iterative routine, we first compute the product $\mathsf{B}\overline{\mathbf{V}}_n$ and obtain a column vector as the result. Then, we right-produce this column vector times matrix S and use the result to refine the iterative solution. A similar procedure may be used to compute the matrix–vector product $\mathsf{A}^T \cdot \overline{\mathbf{V}}_n$ as well.

Notice also that since only products of sparse matrices time vectors are required, and since this operation is not computationally intensive, the routine converges pretty quickly to the solution.

Once the solution of system (11) has been computed, the expansion coefficients for the field that is transmitted into each hole may be found without solving any other linear systems. To this end, we only need to use (9), where matrix $\mathsf{T}^{[p]} = \mathrm{diag}(\mathsf{T}^{[p]}_{-\ell_{\max}}, \mathsf{T}^{[p]}_{-\ell_{\max}+1}, \ldots, \mathsf{T}^{[p]}_{-\ell_{\max}-1}\mathsf{T}^{[p]}_{-\ell_{\max}})$ is a block diagonal matrix, with each of the blocks as in (4).

As a final comment, we remark an important feature of the routine we have presented: since the scattered field is expressed through second-type Hankel functions, and since these functions obey Sommerfeld radiation conditions at infinity, no boundary conditions in the radial coordinate have to be implemented.

IV. Numerical Validation

In order to test the routine, we considered the propagation in a PC waveguide realized in an high-index membrane, and we compared the out-of-plane scattering losses that we computed by using the proposed method and a commercial FDTD routine.

Waveguiding is obtained by assuming that a triangular lattice of air holes is etched in the membrane and that a row of holes is removed, thus forming a linear defect [9]. The pitch and the radius of the holes were chosen so that their suppression permitted opening of a forbidden gap. The following parameters were used: the pitch is $a = 403$ nm, holes' radii are $\rho = 0.3a$, and the membrane thickness and refractive index are $d = 0.6a$ and $n = 3.4$, respectively.

Fig. 3 shows the out-of-plane scattering losses that we computed by means of the FDTD (open circles) and of the proposed routine (solid squares and solid line). In order to obtain these results, we considered a waveguide that contained a number of holes as large as 246 and was formed by 24 elementary cells along the propagation direction (the elementary cell is displayed in the inset of Fig. 3). The flux of the Poynting vector was computed on the edge of cells ranging from the sixth to the eighteenth, and exponentially decaying regression was then used to evaluate the loss. The reason why we did not consider the first and the last six cells is the following: the "cladding" of the PC waveguide confines light in the defect by multiple reflections, interfering in a proper way; for this to occur, a minimum number of elementary cells is required, and near the guide input and output, the field is blurred, compared with the rest of the PC waveguide.

When we used the FDTD, we observed that reliable results could be obtained if the step of the discretization grid was smaller than 10 nm. By exploiting the symmetry with respect to the axis in the middle of the defect waveguide, this implied a

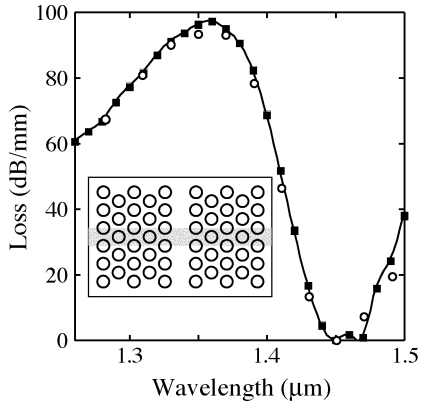

Fig. 3. Out-of-plane scattering losses. Circles: FDTD. Solid squares: The proposed routine. Inset: Top view of the waveguide. The shaded region is the elementary cell.

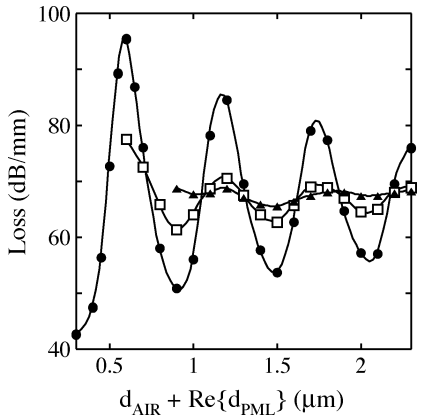

Fig. 4. Dependence of the computed loss on the parameters of the PML. The solid circles refer to a PML thickness $d_{\mathrm{PML}} = 0.3(1 - i0.4)\lambda$, the open squares refer to $d_{\mathrm{PML}} = 0.6(1 - i0.4)\lambda$, and the filled triangles to $d_{\mathrm{PML}} = 0.9(1 - i0.4)\lambda$, respectively. The wavelength is $\lambda = 1280$ nm.

memory occupancy of about 2 GB. Computation time for each wavelength we considered was in the order of 40 h on a 3-GHz processor.

As for the proposed routine, we set $\ell_{\max} = 3$ and $m_{\max} = 55$, respectively, i.e., we used seven azimuthal orders and 55 TE plus 55 TM modes. This way, the field in each hole was expanded over a set of 770 orthogonal functions, and the overall problem contained 94 710 unknowns. Memory occupancy was 800 MB, and the computation time was in the order of 1 h for each point we considered.

Fig. 4 gives some more details on the numerical accuracy of the solution we computed by means of the proposed method. It shows the loss that we computed by changing both the thickness of the air layer above the membrane and that of the PML. The figure abscissa is the overall real thickness of air plus PML. The three curves refer to PML thicknesses equal to $d_{\mathrm{PML}} = 0.3(1 - i0.4)\lambda$ (solid circles), $d_{\mathrm{PML}} = 0.6(1 - i0.4)\lambda$ (open squares), and $d_{\mathrm{PML}} = 0.9(1 - i0.4)\lambda$ (solid triangles), respectively. In these simulations, the wavelength was set equal to $\lambda = 1280$ nm. As it may be observed, the hard boundary that terminates the PML may give rise to unreliable results if an excessively thin PML is chosen.

A general rule for the choice of the optimal PML cannot be given. However, when we tested our code, we noticed that results tend to stabilize for real PML thickness greater than 0.6 λ and imaginary thickness greater than $\lambda/3$.

V. Conclusion

In this paper, a novel numerical method was presented that is particularly suitable for theoretical analysis of 3-D PC waveguides with 2-D arrangements of air holes. The method is a generalization of the multiple-scattering technique developed by Tayeb and Maystre for 2-D PCs. It is based on the representation of the field in the form of sums of cylindrical harmonics, and it fully exploits the fact that, due to the geometrical shape of the objects that make up the PC, relatively few terms are enough to provide a sufficiently accurate field expansion. This reflects in a memory occupancy and computational time that may be significantly lower than those required by other 3-D codes.

Appendix A
On the Modes of a Layered Cavity

Let us consider a cylindrical cavity with several properties.

1) The refractive index in the cavity is independent of both the radial and the azimuthal coordinate, while it is piecewise constant with respect to z.
2) Along z, the cavity contains Q layers, each of which has the thickness d_i and the refractive index n_i. Notice that d_i may be a *complex* number, in which case the corresponding layer is a perfectly matched layer [10]. For later use, we also introduce the following symbol: $D_i = \sum_{j=1}^{i} d_j$.
3) The cavity is closed, on the upper and lower sides, by perfectly magnetic walls.

The aim of this appendix is to show how the modes of such a cavity may be computed and to discuss the relevant properties they have. This task may be carried out by making use of the TE–TM decomposition theorem, which we now recall for the sake of clarity. The theorem states that *in a simply connected region containing a linear isotropic medium, any electromagnetic field* $\{\mathbf{E},\mathbf{H}\}$ *may always be expressed as the sum of two e.m. fields*, $\{\mathbf{E},\mathbf{H}\} = \{\mathbf{E}^{(\mathrm{TE})},\mathbf{H}^{(\mathrm{TE})}\} + \{\mathbf{E}^{(\mathrm{TM})},\mathbf{H}^{(\mathrm{TM})}\}$, *which have the following properties:*

$$\mathbf{E}^{(\mathrm{TE})}\cdot\hat{\boldsymbol{z}} = 0, \quad \mathbf{H}^{(\mathrm{TM})}\cdot\hat{\boldsymbol{z}} = 0.$$

The two fields are obtained from two Debye's potentials, e.g., from two solutions of the scalar homogeneous Helmholtz equation, say L *and* T, *respectively, as follows*:

$$\begin{cases} \mathbf{H}^{(\mathrm{TE})} = \frac{1}{\mu}\left[\left(\frac{\omega}{c}\right)^2 L\hat{\boldsymbol{z}} + \frac{\partial\nabla L}{\partial z}\right] \\ \mathbf{E}^{(\mathrm{TE})} = -i\omega\nabla L\times\hat{\boldsymbol{z}}, \end{cases} \tag{13}$$

$$\begin{cases} \mathbf{E}^{(\mathrm{TM})} = -\frac{1}{\epsilon}\left[\left(\frac{\omega}{c}\right)^2 T\hat{\boldsymbol{z}} + \frac{\partial\nabla T}{\partial z}\right] \\ \mathbf{H}^{(\mathrm{TM})} = -i\omega\nabla T\times\hat{\boldsymbol{z}} \end{cases} \tag{14}$$

with ω *the field frequency and* μ *and* ϵ *the magnetic and electric permittivity, respectively* [15].

Notice that since the cavity we are considering is not a homogeneous medium, but rather a stack of homogenous media, the TE–TM decomposition theorem must be applied separately to each layer. The modes of the whole structure may then be computed by imposing continuity conditions at the layers' interfaces, and as we will see, the whole structure will still admit existence of pure TE and pure TM modes.

A. TE Modes

We take the qth layer in the cavity and consider the homogeneous Helmholtz equation

$$\nabla^2 L_q = \kappa_{\epsilon_q}^2 L_q, \quad D_{q-1}\le z\le D_q. \tag{15}$$

This equation may be solved in a cylindrical reference frame $\{\hat{\boldsymbol{r}},\hat{\boldsymbol{\varphi}},\hat{\boldsymbol{z}}\}$ by using the separation of variables: we introduce the ansatz $L_q = R_q(r)\Phi_q(\varphi)Z_q(z)$ into (15) and get the following system of differential equations:

$$\begin{cases} \frac{d^2R_q}{dr^2} + \frac{1}{r}\frac{dR_q}{dr} + \left(\chi_q^2 - \frac{\ell_q^2}{r^2}\right)R_q = 0 \\ \frac{d^2Z_q}{dz^2} = -k_q^2 Z_q, \quad D_{q-1}\le z\le D_q \\ \frac{d^2\Phi_q}{d\varphi^2} = -\ell_q^2\Phi_q \end{cases} \tag{16}$$

with

$$k_q^2 = \left(\frac{\omega}{c_0}n_q\right)^2 - \chi_q^2. \tag{17}$$

The first of (16) indicates that the radial dependence of L_q is given by either a Bessel or an Hankel function of order ℓ_q. To keep the treatment as general as possible, we write the generic Bessel/Hankel function as $\mathcal{R}_{\ell_q}(r)$ so that

$$L_q = \mathcal{R}_{\ell_q}(\chi_q r)\left[C_q\cos(k_q z) + S_q\sin(k_q z)\right]e^{i\ell_q\varphi} \tag{18}$$

with $\ell_q = \{0,1,2,\ldots\}$.

In this expression, the radial wavenumber χ_q (or, equivalently, the z wavenumber k_q) is an unknown quantity, which may be determined by using the transfer matrix method described in [10].

1) In order for the continuity of transverse components of fields (13) to hold for any value of φ, the azimuthal order ℓ_q must be the same in all the layers: $\ell_q \equiv \ell$, $q = 1,\ldots,Q$.
2) In the same way, for the continuity to be satisfied for any r, also the radial wavenumber χ_q is actually independent on the layer: $\chi_q \equiv \chi$, $q = 1,\ldots,Q$.
3) In the absence of PML, the admissible values of χ form a countable set, a finite number of which is real, and the remaining are purely imaginary, whereas in the presence of PML, all the eigenvalues are complex. The entries of this set may be ordered (for instance, by decreasing real values and increasing imaginary values), and we denote the generic entry in the set as $\chi_m^{(\mathrm{TE})}$.

The explicit form of the TE field components is

$$E_{r,m}^{(\mathrm{TE})} = \frac{\omega\ell}{r}\mathcal{R}_\ell\left(\chi_m^{(\mathrm{TE})}r\right)\mathcal{H}_m(z)e^{i\ell\varphi}$$

$$E_{\varphi,m}^{(\mathrm{TE})} = i\omega\frac{d\mathcal{R}_\ell\left(\chi_m^{(\mathrm{TE})}r\right)}{dr}\mathcal{H}_m(z)e^{i\ell\varphi}$$

$$H_{r,m}^{(\mathrm{TE})} = \frac{1}{\mu_0}\frac{d\mathcal{R}_\ell\left(\chi_m^{(\mathrm{TE})}r\right)}{dr}\frac{d\mathcal{H}_m(z)}{dz}e^{i\ell\varphi}$$
$$H_{\varphi,m}^{(\mathrm{TE})} = \frac{i\ell}{\mu_0 r}\mathcal{R}_\ell\left(\chi_m^{(\mathrm{TE})}r\right)\frac{d\mathcal{H}_m(z)}{dz}e^{i\ell\varphi}$$
$$H_{z,m}^{(\mathrm{TE})} = \frac{\left(\chi_m^{(\mathrm{TE})}\right)^2}{\mu_0}\mathcal{R}_\ell\left(\chi_m^{(\mathrm{TE})}r\right)\mathcal{H}_m(z)e^{i\ell\varphi} \qquad (19)$$

with

$$\mathcal{H}_m(z) = C_q\cos\left[k_q\left(\chi_m^{(\mathrm{TE})}\right)z\right] + S_q\sin\left[k_q\left(\chi_m^{(\mathrm{TE})}\right)z\right]$$

for $D_{q-1} \le z \le D_q$ and $q = 1,\ldots,Q$.

B. TM Modes

TM modes may be found in an analogous way, provided that (14) is used instead of (13). For the sake of brevity, we only quote the final result, which reads

$$E_{r,m}^{(\mathrm{TM})} = -\frac{1}{n^2(z)\epsilon_0}\frac{d\mathcal{R}_\ell\left(\chi_m^{(\mathrm{TM})}r\right)}{dr}\frac{d\mathcal{E}_m(z)}{dz}e^{i\ell\varphi}$$
$$E_{\varphi,m}^{(\mathrm{TM})} = -\frac{i\ell}{n^2(z)\epsilon_0 r}\mathcal{R}_\ell\left(\chi_m^{(\mathrm{TM})}r\right)\frac{d\mathcal{E}_m(z)}{dz}e^{i\ell\varphi}$$
$$E_{z,m}^{(\mathrm{TM})} = -\frac{\left(\chi_m^{(\mathrm{TM})}\right)^2}{n^2(z)\epsilon_0}\mathcal{R}_\ell\left(\chi_m^{(\mathrm{TM})}r\right)\mathcal{E}_m(z)e^{i\ell\varphi}$$
$$H_{r,m}^{(\mathrm{TM})} = \frac{\omega\ell}{r}\mathcal{R}_\ell\left(\chi_m^{(\mathrm{TM})}r\right)\mathcal{E}_m(z)e^{i\ell\varphi}$$
$$H_{\varphi,m}^{(\mathrm{TM})} = i\omega\chi_m^{(\mathrm{TM})}\frac{d\mathcal{R}_\ell\left(\chi_m^{(\mathrm{TM})}r\right)}{dr}\mathcal{E}_m(z)e^{i\ell\varphi}. \qquad (20)$$

C. On the Radial Dependence of the Modes

In this previous derivation, we kept the radial dependence of the field as general as possible. Now, we look at the point with some more detail, and we clarify the circumstances under which $\mathcal{R}$ specializes as a Bessel or an Hankel function.

The theory we have developed applies to any layered medium. Thus, it may be used to represent a field in both the holes or in the slab waveguide. In the former case, the cavity domain is a finite region that includes the origin of the cylindrical reference frame. Then, the field may only contain J-type Bessel functions. By contrast, in the latter case, one must distinguish among two cases. As a matter of fact, the expansion in the slab region may be used to represent both the field that is injected toward the holes, i.e., the field that *impinges* on the PC, or the field that is scattered by the holes. The scattered field must obey Sommerfeld radiation conditions. Hence, it must be expressed through a second-type Hankel function.[1] By virtue of the induction theorem, on the other hand, the incident field may always be expressed by means of J-type Bessel functions only [11].

[1]Second-type Hankel functions are outgoing waves for time-harmonic fields of the type $\mathbf{e}(t) = \mathrm{Re}\{\mathbf{E}\exp(i\omega t)\}$. If the complex vector were defined through the kernel $\exp(-i\omega t)$, the first-type Hankel functions had to be used instead.

D. Properties of Functions $\mathcal{H}(\cdot)$ and $\mathcal{E}(\cdot)$

We now show that if we take any couple of nondegenerate modes, i.e., modes with radial wavenumbers $\chi_m^2 \neq \chi_p^2$, the following properties hold:

$$\langle\mathcal{H}_m|\mathcal{H}_p\rangle \equiv \int_0^{D_Q}\mathcal{H}_m(z)\mathcal{H}_p^*(z)dz = \langle\mathcal{H}_m|\mathcal{H}_m\rangle\delta_{mp} \qquad (21)$$

$$\left\langle\mathcal{E}_m\left|\frac{1}{n^2}\right|\mathcal{E}_p\right\rangle \equiv \int_0^{D_Q}\frac{\mathcal{E}_m(z)\mathcal{E}_p^*(z)}{n^2(z)}dz = \left\langle\mathcal{E}_m\left|\frac{1}{n^2}\right|\mathcal{E}_m\right\rangle\delta_{mp} \qquad (22)$$

$$\mathcal{I}[\mathcal{E}_m,\mathcal{H}_p] = \int_0^{D_Q}\frac{1}{n^2(z)}\left[\left(\chi_m^{(\mathrm{TM})}\right)^2\mathcal{E}_m(z)\frac{d\mathcal{H}_p^*(z)}{dz} + \left(\chi_p^{*(\mathrm{TE})}\right)^2\mathcal{H}_p^*(z)\frac{d\mathcal{E}_m(z)}{dz}\right]dz = 0. \qquad (23)$$

To prove the statements, we consider the first of these equations and rewrite the integral as

$$\langle\mathcal{H}_m|\mathcal{H}_p\rangle = \sum_{i=1}^{Q}\int_{D_{i-1}}^{D_i}\mathcal{H}_m(z)\mathcal{H}_p^*(z)dz.$$

In addition, we introduce the quantity

$$I_i = \int_{D_{i-1}}^{D_i}\left(\mathcal{H}_m(z)\frac{d^2\mathcal{H}_p^*(z)}{dz^2} - \frac{d^2\mathcal{H}_m(z)}{dz^2}\mathcal{H}_p^*(z)\right)dz.$$

Since within each layer $\mathcal{H}(\cdot) \in C^\infty_{(D_{i-1},D_i)}$, we may integrate by parts to obtain

$$I_i = \left[\mathcal{H}_m(z)\frac{d\mathcal{H}_p^*(z)}{dz} - \frac{d\mathcal{H}_m(z)}{dz}\mathcal{H}_p^*(z)\right]_{z=D_{i-1}^+}^{z=D_i^-}.$$

On the other hand, using (16) and (17), we also get

$$I_i = \left[\left(k_{p_i}^*\right)^2 - k_{m_i}^2\right]\int_{D_{i-1}}^{D_i}\mathcal{H}_m(z)\mathcal{H}_p^*(z)dz = \left[\chi_m^2 - \left(\chi_p^*\right)^2\right]\int_{D_{i-1}}^{D_i}\mathcal{H}_m(z)\mathcal{H}_p^*(z)dz.$$

Then, since χ_m^2 and χ_p^2 do not depend on the layer, i.e., they do not depend on z, we find

$$\langle\mathcal{H}_m|\mathcal{H}_p\rangle = \frac{\sum_{i=1}^{Q}\left[\mathcal{H}_m(z)\frac{d\mathcal{H}_p^*(z)}{dz} - \frac{d\mathcal{H}_m(z)}{dz}\mathcal{H}_p^*(z)\right]_{z=D_{i-1}^+}^{z=D_i^-}}{\left[\chi_m^2 - \left(\chi_p^*\right)^2\right]}$$

so that, being $\chi_m^2 \neq \chi_p^2$ by hypothesis, (21) is actually proven if we show that

$$\sum_{i=1}^{Q}\left[\mathcal{H}_m(z)\frac{d\mathcal{H}_p^*(z)}{dz}-\frac{d\mathcal{H}_m(z)}{dz}\mathcal{H}_p^*(z)\right]_{z=D_{i-1}^+}^{z=D_i^-}=0.$$

This is done as follows. From (19), we see that the functions $\mathcal{H}(z)$ and $d\mathcal{H}/dz$ are proportional to the transverse components of the electric and magnetic fields of a TE mode, respectively. Then, the addendum in the sum vanishes for $z=0^+$ and $z=D_Q^-$ since the upper and lower edges of the cavity are perfectly magnetic walls, whereas electric-field continuity through the layers implies that any term that is evaluated in $z=D_i^-$ cancels out with the one in $z=D_i^+$. In this way, the overall quantity sums to zero, thereby proving (21) indeed.

Proof of (22) and (23) may be carried out in an analogous fashion, and it is left to the reader for the sake of brevity.

E. Orthogonality Properties

As a closing remark on the modes of a layered cavity, we now prove some relevant orthogonality relationships. We denote as $\{\mathbf{E}_h^{(\mathrm{TE})},\mathbf{H}_h^{(\mathrm{TE})}\}$, $\{\mathbf{E}_k^{(\mathrm{TE})},\mathbf{H}_k^{(\mathrm{TE})}\}$ a couple of TE modes where h and k stand for $\{m,\ell\}$ and $\{m',\ell'\}$, respectively. The following orthogonality relationship is found:

$$\begin{aligned}&\iint_S\left(\mathbf{E}_h^{(\mathrm{TE})}\times\mathbf{H}_k^{*(\mathrm{TE})}\right)\cdot\hat{\boldsymbol{r}}dS=F_h\delta_{hk}\\&F_h=\frac{2\pi i\omega}{\mu_0}\chi_h^{(\mathrm{TE})}\left(\chi_h^{*(\mathrm{TE})}\right)^2\\&\qquad\cdot\mathcal{R}_\ell'\left(\chi_h^{(\mathrm{TE})}r\right)\left[\mathcal{R}_\ell\left(\chi_h^{(\mathrm{TE})}r\right)\right]^*\langle\mathcal{H}_h|\mathcal{H}_h\rangle\end{aligned}\tag{24}$$

where S is any cylindrical surface parallel to the z axis.

The proof stems directly from (21). In fact, using (19) and (20), we recognize that the integral $\langle\mathcal{H}_m|\mathcal{H}_p\rangle$ may be factored out in the RHS of (24), and the relationship is then immediately proved.

In a similar fashion, if $\{\mathbf{E}_h^{(\mathrm{TM})},\mathbf{H}_h^{(\mathrm{TM})}\}$, $\{\mathbf{E}_k^{(\mathrm{TM})},\mathbf{H}_k^{(\mathrm{TM})}\}$ are two TM modes, from (22), it also follows that

$$\begin{aligned}&\iint_S\left(\mathbf{E}_h^{(\mathrm{TM})}\times\mathbf{H}_k^{*(\mathrm{TM})}\right)\cdot\hat{\boldsymbol{r}}dS=G_h\delta_{hk}\\&G_h=\frac{2\pi i\omega}{\epsilon_0}\chi_h^{*(\mathrm{TM})}\left(\chi_h^{(\mathrm{TM})}\right)^2\\&\qquad\cdot\left[\mathcal{R}_\ell'\left(\chi_h^{(\mathrm{TM})}r\right)\right]^*\mathcal{R}_\ell\left(\chi_h^{(\mathrm{TM})}r\right)\left\langle\mathcal{E}_h\left|\frac{1}{n^2}\right|\mathcal{E}_h\right\rangle.\end{aligned}\tag{25}$$

Finally, every couple $\{\mathbf{E}_h^{(\mathrm{TE})},\mathbf{H}_h^{(\mathrm{TE})}\}$, $\{\mathbf{E}_k^{(\mathrm{TM})},\mathbf{H}_k^{(\mathrm{TM})}\}$ satisfies the relations

$$\iint_S\left(\mathbf{E}_h^{(\mathrm{TE})}\times\mathbf{H}_k^{*(\mathrm{TM})}\right)\cdot\hat{\boldsymbol{r}}dS=0\tag{26}$$

$$\iint_S\left(\mathbf{E}_k^{(\mathrm{TM})}\times\mathbf{H}_h^{*(\mathrm{TE})}\right)\cdot\hat{\boldsymbol{r}}dS=0.\tag{27}$$

APPENDIX B
FORM OF ENTRIES IN (2)

The explicit expression of entries in (2) are the following:

$$\begin{aligned}\mathsf{M}_{11}(p,m)=&\,\omega\left(\chi_{\mathrm{SL}p}^{*(\mathrm{TE})}\right)^2\chi_{\mathrm{SL}m}^{(\mathrm{TE})}H_\ell'^{(2)}\left(\chi_{\mathrm{SL}m}^{(\mathrm{TE})}\rho\right)\\&\cdot\langle\mathcal{H}_m^{\mathrm{SL}}|\mathcal{H}_p^{\mathrm{SL}}\rangle\\\mathsf{M}_{13}(p,m)=&-\omega\left(\chi_{\mathrm{SL}p}^{*(\mathrm{TE})}\right)^2\chi_{\mathrm{HO}m}^{(\mathrm{TE})}J_\ell'\left(\chi_{\mathrm{HO}m}^{(\mathrm{TE})}\rho\right)\\&\cdot\langle\mathcal{H}_m^{\mathrm{HO}}|\mathcal{H}_m^{\mathrm{SL}}\rangle\\\mathsf{M}_{14}(p,m)=&\frac{\ell}{\epsilon_0\rho}J_\ell\left(\chi_{\mathrm{HO}m}^{(\mathrm{TM})}\rho\right)\mathcal{I}\left[\mathcal{E}_m^{\mathrm{HO}},\mathcal{H}_p^{\mathrm{SL}}\right]\\\mathsf{M}_{22}(p,m)=&\left(\chi_{\mathrm{SL}m}^{(\mathrm{TM})}\right)^2H_\ell^{(2)}\left(\chi_{\mathrm{SL}m}^{(\mathrm{TM})}\rho\right)\\&\cdot\left\langle\mathcal{E}_m^{\mathrm{SL}}\left|\frac{1}{n_{\mathrm{SL}}^2}\right|\mathcal{E}_p^{\mathrm{SL}}\right\rangle\\\mathsf{M}_{24}(p,m)=&-\left(\chi_{\mathrm{HO}m}^{(\mathrm{TM})}\right)^2J_\ell\left(\chi_{\mathrm{HO}m}^{(\mathrm{TM})}\rho\right)\\&\cdot\left\langle\mathcal{E}_m^{\mathrm{HO}}\left|\frac{1}{n_{\mathrm{HO}}^2}\right|\mathcal{E}_p^{\mathrm{SL}}\right\rangle\\\mathsf{M}_{31}(p,m)=&\left(\chi_{\mathrm{SL}m}^{(\mathrm{TE})}\right)^2H_\ell^{(2)}\left(\chi_{\mathrm{SL}m}^{(\mathrm{TE})}\rho\right)\cdot\langle\mathcal{H}_m^{\mathrm{SL}}|\mathcal{H}_p^{\mathrm{SL}}\rangle\\\mathsf{M}_{33}(p,m)=&-\left(\chi_{\mathrm{HO}m}^{(\mathrm{TE})}\right)^2J_\ell\left(\chi_{\mathrm{HO}m}^{(\mathrm{TE})}\rho\right)\cdot\langle\mathcal{H}_m^{\mathrm{HO}}|\mathcal{H}_p^{\mathrm{SL}}\rangle\\\mathsf{M}_{42}(p,m)=&\,\omega\left(\chi_{\mathrm{SL}p}^{*(\mathrm{TM})}\right)^2\chi_{\mathrm{SL}m}^{(\mathrm{TM})}H_\ell'^{(2)}\left(\chi_{\mathrm{SL}m}^{(\mathrm{TM})}\rho\right)\\&\cdot\left\langle\mathcal{E}_m^{\mathrm{SL}}\left|\frac{1}{n_{\mathrm{SL}}^2}\right|\mathcal{E}_p^{\mathrm{SL}}\right\rangle\\\mathsf{M}_{43}(p,m)=&-\frac{\ell}{\mu_0\rho}J_\ell\left(\chi_{\mathrm{HO}m}^{(\mathrm{TE})}\rho\right)\mathcal{I}\left[\mathcal{E}_p^{\mathrm{SL}},\mathcal{H}_m^{\mathrm{HO}}\right]^*\\\mathsf{M}_{44}(p,m)=&-\omega\left(\chi_{\mathrm{SL}p}^{*(\mathrm{TM})}\right)\chi_{\mathrm{HO}m}^{(\mathrm{TM})}J_\ell'\left(\chi_{\mathrm{HO}m}^{(\mathrm{TM})}\rho\right)\\&\cdot\left\langle\mathcal{E}_m^{\mathrm{HO}}\left|\frac{1}{n_{\mathrm{SL}}^2}\right|\mathcal{E}_p^{\mathrm{SL}}\right\rangle\end{aligned}$$

whereas

$$\begin{aligned}\mathbf{P}_1(p)=&-\omega\left(\chi_{\mathrm{SL}p}^{*(\mathrm{TE})}\right)^2\sum_m\chi_{\mathrm{SL}m}^{(\mathrm{TE})}L_{\ell,m}^{(i)}J_\ell'\left(\chi_{\mathrm{SL}m}^{(\mathrm{TE})}\rho\right)\\&\cdot\langle\mathcal{H}_m^{\mathrm{SL}}|\mathcal{H}_p^{\mathrm{SL}}\rangle\\\mathbf{P}_2(p)=&-\sum_m\left(\chi_{\mathrm{SL}m}^{(\mathrm{TM})}\right)^2T_{\ell,m}^{(i)}J_\ell\left(\chi_{\mathrm{SL}m}^{(\mathrm{TM})}\rho\right)\\&\cdot\left\langle\mathcal{E}_m^{\mathrm{SL}}\left|\frac{1}{n_{\mathrm{SL}}^2}\right|\mathcal{E}_p^{\mathrm{SL}}\right\rangle\\\mathbf{P}_3(p)=&-\sum_m\left(\chi_{\mathrm{SL}m}^{(\mathrm{TE})}\right)^2L_{\ell,m}^{(i)}J_\ell\left(\chi_{\mathrm{SL}m}^{(\mathrm{TE})}\rho\right)\cdot\langle\mathcal{H}_m^{\mathrm{SL}}|\mathcal{H}_p^{\mathrm{SL}}\rangle\\\mathbf{P}_4(p)=&-\omega\left(\chi_{\mathrm{SL}p}^{*(\mathrm{TM})}\right)^2\sum_m\chi_{\mathrm{SL}m}^{(\mathrm{TM})}T_{\ell,m}^{(i)}J_\ell'\left(\chi_{\mathrm{SL}m}^{(\mathrm{TM})}\rho\right)\\&\cdot\left\langle\mathcal{E}_m^{\mathrm{SL}}\left|\frac{1}{n_{\mathrm{SL}}^2}\right|\mathcal{E}_p^{\mathrm{SL}}\right\rangle.\end{aligned}$$

Finally

$$\mathsf{P}_{11}(p,m) = -\omega\left(\chi_{\mathrm{SL}p}^{*(\mathrm{TE})}\right)^2 \chi_{\mathrm{SL}m}^{(\mathrm{TE})} J_\ell'\left(\chi_{\mathrm{SL}m}^{(\mathrm{TE})}\rho\right)\langle \mathcal{H}_m^{\mathrm{SL}} | \mathcal{H}_p^{\mathrm{SL}}\rangle$$

$$\mathsf{P}_{22}(p,m) = -\left(\chi_{\mathrm{SL}m}^{(\mathrm{TM})}\right)^2 J_\ell\left(\chi_{\mathrm{SL}m}^{(\mathrm{TM})}\rho\right)\left\langle \mathcal{E}_m^{\mathrm{SL}} \left| \frac{1}{n_{\mathrm{SL}}^2} \right| \mathcal{E}_p^{\mathrm{SL}} \right\rangle$$

$$\mathsf{P}_{31}(p,m) = -\left(\chi_{\mathrm{SL}m}^{(\mathrm{TE})}\right)^2 J_\ell\left(\chi_{\mathrm{SL}m}^{(\mathrm{TE})}\rho\right)\langle \mathcal{H}_m^{\mathrm{SL}} | \mathcal{H}_p^{\mathrm{SL}}\rangle$$

$$\mathsf{P}_{42}(p,m) = -\omega\left(\chi_{\mathrm{SL}p}^{*(\mathrm{TM})}\right)^2 \chi_{\mathrm{SL}m}^{(\mathrm{TM})} J_\ell'\left(\chi_{\mathrm{SL}m}^{(\mathrm{TM})}\rho\right) \times \left\langle \mathcal{E}_m^{\mathrm{SL}} \left| \frac{1}{n_{\mathrm{SL}}^2} \right| \mathcal{E}_p^{\mathrm{SL}} \right\rangle.$$

ACKNOWLEDGMENT

The authors wish to thank C. G. Someda and B. Tromborg for their discussions.

REFERENCES

[1] E. Yablonovitch, "Photonic band-gap structures," *J. Opt. Soc. Amer. B, Opt. Phys.*, vol. 10, pp. 283–295, 1993.

[2] T. F. Krauss, R. M. De La Rue, and S. Brand, "Two-dimensional photonic bandgap structures operating at near-infrared wavelengths," *Nature*, vol. 383, pp. 699–702, 1996.

[3] J. D. Joannopoulos, P. R. Villeneuve, and S. Fan, "Photonic crystals: Putting a new twist on light," *Nature*, vol. 387, pp. 143–149, 1997.

[4] D. Labilloy, H. Benitsy, C. Weisbuch, T. F. Krauss, R. M. De La Rue, V. Bardinal, R. Houdré, U. Oesterle, D. Cassagne, and C. Jouanin, "Quantitative measurement of transmission, reflection, and diffraction of two-dimensional photonic band gap structures at near-infrared wavelengths," *Phys. Rev. Lett.*, vol. 79, pp. 4147–4150, 1997.

[5] T. F. Krauss and R. M. De La Rue, "Photonic crystals in the optical regime—Past, present and future," *Prog. Quantum Electron.*, vol. 23, pp. 51–96, 1999.

[6] S. G. Johnson, P. R. Villeneuve, S. Fan, and J. D. Joannopouols, "Linear waveguides in photonic-crystal slabs," *Phys. Rev. B, Condens. Matter*, vol. 62, pp. 8212–8222, 2000.

[7] A. Taflove, *Computational Electrodynamics. The Finite Difference Time Domain Method*. Norwood, MA: Artech House, 1995.

[8] M. Paulus and O. J. F. Martin, "Light propagation and scattering in stratified media: A Green's tensor approach," *J. Opt. Soc. Amer. A, Opt. Image Sci.*, vol. 18, pp. 854–861, 2001.

[9] P. Lalanne, "Electromagnetic analysis of photonic crystal waveguides operating above the light cone," *IEEE J. Quantum Electron.*, vol. 38, pp. 800–804, July 2002.

[10] P. Bienstman and R. Baets, "Advanced boundary conditions for eigenmode expansion models," *Opt. Quantum Electron.*, vol. 34, pp. 523–540, 2002.

[11] G. Tayeb and D. Maystre, "Rigorous theoretical study of finite-size two-dimensional photonic crystals doped by microcavities," *J. Opt. Soc. Amer. A, Opt. Image Sci.*, vol. 14, pp. 3323–3332, 1997.

[12] M. Abramowitz and I. Stegun, *Handbook of Mathematical Functions*. New York: Dover , 1964.

[13] K. A. Zaki, S. W. Chen, and C. Chen, "Modeling discontinuities in dielectric-loaded waveguides," *IEEE Trans. Microwave Theory Tech.*, vol. 36, pp. 1804–1810, Dec. 1988.

[14] D. Young, *Iterative Solution of Large Linear Systems*. New York: Academic, 1971.

[15] C. G. Someda, *Electromagnetic Waves*. London, U.K.: Chapman & Hall, 1998.

Stefano Boscolo was born in Chioggia, Italy, in 1974. He received the Laurea degree (*cum laude*) in electronic engineering from the University of Padova, Padova, Italy, in 1999. He is currently working toward the Ph.D. degree at the University of Udine, Udine, Italy.

His fields of technical interest focus on the numerical and theoretical analysis of electromagnetic-wave propagation in photonic crystals and the modeling and design of integrated optical devices.

Michele Midrio was born in Padova, Italy, in 1967. He received the Laurea degree (*cum laude*) in electronic engineering and the Ph.D. degree in telecommunications from the University of Padova, Padova, Italy, in 1991 and 1994, respectively.

He was with the Fondazione Ugo Bordoni, Rome, Italy, from 1993 to 1996, where he worked on optical fiber communications. He is currently a Professor of electromagnetic fields at the University of Udine, Udine, Italy. He has authored or coauthored approximately 100 papers and conference contributions and holds four patents. His field of technical interest focuses on optical communications, soliton propagation, and photonics.

Dr. Midrio received the Philip Morris award for scientific research in the area of information technology and telecommunications in 1993.